Analysis of Sampled-Data Hybrid Integrator-Gain Systems: A Discrete-Time Approach ⋆

B. Sharif [a], D.W.T. Alferink [a], M.F. Heertjes [a,b], H. Nijmeijer [a], W.P.M.H. Heemels [a]

[a] *Department of Mechanical Engineering, Eindhoven University of Technology, 5600 MB, Eindhoven, The Netherlands*

[b] *Mechatronics System Development, ASML, 5504 DR, Veldhoven, The Netherlands*

Abstract

Hybrid integrator-gain systems (HIGS) are hybrid control elements used to overcome fundamental performance limitations of linear time-invariant feedback control, and have enjoyed recent successes in engineering applications such as high-precision motion systems. However, despite the relevance of digital implementations, the creation of sampled-data versions of HIGS and their formal analysis have not been addressed in the literature so far, and will form the topic of the present paper. Thereto, we present discrete-time HIGS elements, which preserve the main philosophy behind the operation of HIGS in continuous time. Moreover, stability criteria are presented that can be used to certify input-to-state stability of discrete-time and sampled-data HIGS-controlled systems based on both (i) (measured) frequency response data, and (ii) linear matrix inequalities (LMIs). A comparison between these stability criteria is presented as well. A numerical case study is provided to illustrate the application of the main results.

Key words: Hybrid integrator-gain systems; Sampled-data systems; Stability Analysis.

1 Introduction

Hybrid integrator-gain systems (HIGS) are hybrid control elements that have been shown to be effective in overcoming fundamental limitations of linear time-invariant (LTI) control [31, 33]. Extensive research has led to several fruitful results for HIGS-based control design in terms of mathematical formalization, well-posedness and stability analysis [6, 26, 27], improving closed-loop performance of control systems, mainly in the context of high-precision motion control [5, 28, 32], but also for the consensus of multiagent systems [35]. In addition, in [31, 33] it has been formally shown that well-known fundamental limitations of LTI feedback control wherein overshoot in the step response of the system is unavoidable for any stabilizing LTI controller, can indeed be overcome using HIGS-based control. Finally, let us stress a particularly desirable feature of HIGS, as characterized by its describing function [5], which is a 20 dB/decade amplitude decay similar to that of a linear integrator, while inducing only 38.15 degrees of phase lag (as opposed to 90 degrees in the linear case). In turn, this improvement in terms of phase lag hints towards the possibility of designing controllers capable of achieving the desired closed-loop bandwidth with a much reduced gain at higher frequencies, thereby improving closed-loop performance.

Thus far, the literature related to HIGS has predominantly focused on *continuous-time* (CT) HIGS-controlled systems. Obviously, in practice, almost all controllers are implemented digitally and thus in *discrete time* (DT). This leads to a closed-loop configuration consisting of CT plants, e.g., a high precision motion system, to be controlled by DT controllers (and sample and hold elements), and thus, an overall *sampled-data* (SD) control system. In this paper, we aim to address important aspects related to the creation of proper SD implementations of HIGS-based controllers and their analysis, which are missing in the current literature ex-

⋆ This work has received funding from the European research council (ERC) through the Advanced Grant Proactive, no. 10105538, and the Dutch research council (NWO) through the CLOC project. Views and opinions expressed are however those of the author(s) only and do not necessarily reflect those of the European Union or the European Research Council. Neither the European Union nor the granting authority can be held responsible for them.

Email addresses: b.sharif@tue.nl (B. Sharif), d.w.t.alferink@student.tue.nl (D.W.T. Alferink), M.F.Heertjes@tue.nl (M.F. Heertjes), h.nijmeijer@tue.nl (H. Nijmeijer), w.p.m.h.heemels@tue.nl (W.P.M.H. Heemels).

cept for our preliminary conference version [25] of this work.

Generally speaking, a large body of literature is available for SD control, see, e.g., [2,4,8,9], from which three main approaches can be distinguished. These are [20]:

(1) the continuous-time design approach (abbreviated as CTD), in which CT controllers are designed based on a CT model of the plant and the obtained CT controllers are subsequently discretized and implemented;
(2) the discrete-time approach (abbreviated as DTD), in which a discrete-time (DT) controller is designed based on a DT model of the plant;
(3) the sampled-data design approach (abbreviated as SDD), in which a discrete-time controller is directly designed based on a CT model of the plant.

In the CTD approach, while one can benefit from CT (physical)design/analysis insights and tools, the digital controller implementation is not considered. To make the CTD work, there is a need for a digital implementation that approaches the behavior of the (designed) CT controller well. In the literature this approach is also referred to as emulation. In particular one needs a (i) high sampling rate, and (ii) a *consistent* discretization of the CT controller [1, 11, 12, 23, 30] such that the solutions to the DT controller are close to the solutions of the controller designed in CT, under fast sampling. While fast sampling could be achieved by (expensive) hardware, consistent discretization of HIGS, being a hybrid controller with a discontinuous vector field, is not straightforward. The SDD approach (see, e.g., [2, 13]) does not consider an "approximate" CT model of the implemented digital controller (as in the CTD approach) and includes the inter-sample plant behavior in the analysis and design (as opposed to the DTD approach). However, it is the most complex approach among the three due to the hybrid nature of the system it considers. Additionally, SDD methods require CT plant models, which are not always readily available. In many applications, such as control of high precision motion systems, the plant model is often obtained by means of data-driven methods and thus evolves in DT. Therefore, using SDD methods for such applications is not always a well justified choice [22].

In this paper, motivated also by the reasons above, we present tools for the analysis of SD HIGS-controlled systems based on the DTD approach, which is typically easier to apply in practice compared to the SDD approach, and can be used in conjunction with DT models obtained from system identification. Moreover, DTD methods have the advantage of providing direct guarantees on DT closed-loop behavior (in contrast to the CTD approach) involving the size of the sampling period in the analysis and design conditions that can also be used to provide guarantees when taking the inter-sample behavior into account [21]. The latter will be discussed in this paper as well.

In summary, our contributions are fourfold. As a first contribution, we present two DT versions of HIGS, which preserve the essential characteristics and the main philosophy behind the operation of CT HIGS. As a second and third contribution we present two different stability criteria that can be used to certify input-to-state stability (ISS) of systems consisting of DT HIGS-based controllers and a DT LTI plant. These two ISS criteria are based on (i) (measured DT) frequency response data, and (ii) linear matrix inequalities (LMIs). We also show that the LMIs are guaranteed to provide less conservative results compared to the frequency-domain criterion as satisfaction of the latter implies feasibility of a special case of the LMIs. As a fourth and final contribution, it is shown that DT ISS implies also ISS of sampled-data HIGS-controlled systems consisting of DT HIGS-based controllers and a CT LTI plant (including the inter-sample behavior). A numerical case study is also provided to illustrate the results.

The remainder of this paper is organized as follows. Section 2 contains preliminary material and a short introduction to CT HIGS and its main motivation. Section 3 introduces our proposed DT HIGS. In Section 4 the closed-loop system under consideration as well as stability criteria in frequency- and time-domain are presented. Section 5 extends the DT stability analysis to sampled-data HIGS-controlled systems. This is followed by a numerical example and conclusions in Sections 6 and 7, respectively.

2 Preliminaries

In this section, we present some preliminary material that is needed in the sequel.

2.1 Notation and definitions

We note that a matrix $A \in \mathbb{R}^{n\times n}$ is symmetric by $A \in \mathbb{S}^{n\times n}$. Given a symmetric matrix $A \in \mathbb{S}^{n\times n}$ we say that it is positive(negative)-definite, denoted by $A \succ (\prec) 0$, if $x^\top Ax > (<)\ 0$ for all $x \in \mathbb{R}^n \setminus \{0\}$. We write $A \in \mathbb{S}^{n\times n}_{\geq 0}$, if A is symmetric and all its elements are non-negative. The inequality symbols $>,\ \geq,\ <,\ \leq$ for a vector are understood component-wise. For a vector $x \in \mathbb{R}^n$ we denote its p norm in $\mathbb{R}^n$ by $\|x\|_p$. We write $\|x\|$ for the standard Euclidean norm. For a matrix $A \in \mathbb{R}^{n\times m}$, we use $\|A\|_\infty := \max_{1\leq i\leq m} \sum_{j=1}^{n} |a_{ij}|$, where $|a_{ij}|$ denotes the absolute value of the element in the i^{th} row and j^{th} column of A. For a bounded function $u : \mathbb{R}_{\geq 0} \to \mathbb{R}^n$, we write $\|u\|_\infty = \sup_{t\in\mathbb{R}_{\geq 0}} \|u(t)\|$. Similarly for a bounded function $w : \mathbb{N} \to \mathbb{R}^n$ we use the notation $\|w\|_\infty = \sup_{k\in\mathbb{N}} \|w(k)\|$.

Preprint submitted to Automatica
Received November 20, 2023 08:38:48 Pacific Time

Definition 1. *[17] A function $\alpha : [0, a) \to [0, \infty)$ is said to belong to class $\mathcal{K}$, if it is continuous, strictly increasing and $\alpha(0) = 0$, it is a $\mathcal{K}_\infty$ function if it belongs to class $\mathcal{K}$ and $\alpha(s) \to \infty$ as $s \to \infty$. A function $\beta : [0, a) \times [0, \infty) \to [0, \infty)$ is said to belong to class $\mathcal{KL}$, if, it is continuous and for each fixed s, the mapping $r \mapsto \beta(r, s)$ belongs to class $\mathcal{K}$ with respect to r and, for each fixed r, the mapping $s \mapsto \beta(r, s)$ is decreasing with respect to s and $\beta(r, s) \to 0$ as $s \to \infty$.*

Consider a system of the form

$$x[k] = f(x[k-1], w[k-1]) \tag{1}$$

with $x[k]$ taking values in $\mathbb{R}^n$ and $w[k]$ taking values in $\mathbb{R}^m$, denoting the state and input, respectively, at discrete time $k \in \mathbb{N}$. Moreover, $f : \mathbb{R}^n \times \mathbb{R}^m \to \mathbb{R}^n$ is a function satisfying $f(0, 0) = 0$.

Definition 2. *[16] System (1) is said to be input-to-state stable (ISS) with respect to w, if there exist a $\mathcal{KL}$-function $\beta : \mathbb{R}_{\geq 0} \times \mathbb{R}_{\geq 0} \to \mathbb{R}_{\geq 0}$ and a $\mathcal{K}$-function γ such that, for each bounded input $w : \mathbb{N} \to \mathbb{R}^m$ and each initial condition x_0, it holds that*

$$\|x[k, x_0, w]\| \leq \beta(\|x_0\|, k) + \gamma(\|w\|_\infty),$$

for each $k \in \mathbb{N}$, where $x[k, x_0, w]$ denotes the state of system (1), for initial state $x[0] = x_0$ and input w at discrete-time instant k.

Definition 3. *[10, 16] A function $V : \mathbb{R}^n \to \mathbb{R}$ is called an ISS Lyapunov function for the system (1), if the following holds:*

(1) There exist $\mathcal{K}_\infty$-functions α_1 and α_2 such that for all $x \in \mathbb{R}^n$

$$\alpha_1(\|x\|) \leq V(x) \leq \alpha_2(\|x\|). \tag{2}$$

(2) There exist a $\mathcal{K}_\infty$-function α_3 and a $\mathcal{K}$-function γ, such that

$$V(f(x, w)) - V(x) \leq -\alpha_3(\|x\|) + \gamma(\|w\|) \tag{3}$$

for all $x \in \mathbb{R}^n$ and all $w \in \mathbb{R}^m$.

Theorem 1. *The system (1) is ISS in the sense of Definition 3, if it admits an ISS Lyapunov function as defined in Definition 3.*

Proof. See [10, 16] for the proof. □

2.2 Continuous-time HIGS

A CT HIGS element [5], denoted by $\mathscr{H}$, is described by

$$\mathscr{H} : \begin{cases} \dot{x}_h(t) = \omega_h e(t) & \text{if } (e(t), u(t), \dot{e}(t)) \in \mathscr{F}_1, \quad (4a) \\ x_h(t) = k_h e(t) & \text{if } (e(t), u(t), \dot{e}(t)) \in \mathscr{F}_2, \quad (4b) \\ u(t) = x_h(t) & \quad (4c) \end{cases}$$

with state $x_h(t) \in \mathbb{R}$, input $e(t) \in \mathbb{R}$, time-derivative $\dot{e}(t) \in \mathbb{R}$ of the input, and output $u(t) \in \mathbb{R}$, at time $t \in \mathbb{R}_{\geq 0}$. The parameters $\omega_h \in [0, \infty)$ and $k_h \in (0, \infty)$ denote the integrator frequency and the gain parameter of the HIGS element, respectively. Moreover, $\mathscr{F}_1$ and $\mathscr{F}_2$ denote the regions in $\mathbb{R}^3$, where the different subsystems are active. A HIGS element primarily operates in the so-called integrator mode (4a). However, the integrator mode dynamics can only be followed as long as the input-output pair (e, u) of $\mathscr{H}$ remains inside the sector

$$\mathcal{S} := \left\{ (e, u) \in \mathbb{R}^2 \mid eu \geq \frac{1}{k_h} u^2 \right\}. \tag{5}$$

A visual illustration of the set $\mathcal{S}$ is provided in Fig. 2 in Section 3.2 below. When the pair (e, u) tends to leave $\mathcal{S}$, a switch is made to the so-called gain mode (4b), keeping the trajectories on the sector boundary, where $u = k_h e$, and thus in $\mathcal{S}$. In particular, the sets $\mathscr{F}_1$ and $\mathscr{F}_2$, are given by

$$\begin{aligned} \mathscr{F}_2 := \{ &(e, u, \dot{e}) \in \mathbb{R}^3 \mid (e, u) \in \mathcal{S} \wedge u = k_h e \\ &\wedge \omega_h e^2 > k_h \dot{e} e \}, \end{aligned} \tag{6}$$

$$\mathscr{F}_1 := \{(e, u, \dot{e}) \in \mathbb{R}^3 \mid (e, u) \in \mathcal{S}\} \setminus \mathscr{F}_2. \tag{7}$$

As a result of this construction, the sector $\mathcal{S}$ is a forward invariant set for the input-output pair (e, u) of a HIGS element, which results in e and u having the same sign at all times. This feature leads to favorable properties in terms of the reduced phase lag of 38.15 degrees from a describing function perspective [6], in contrast to the 90 degrees phase lag of a standard linear integrator, as was already indicated in the introduction. In [31, 33], it was shown how these features of sign equivalence can be used to overcome fundamental performance limitations present in LTI control, making HIGS a promising control element. Additionally, HIGS has been shown to offer performance enhancing properties, for applications such as high-precision mechatronics [5, 32]. In [6], HIGS have been mathematically formalized in the framework of extended projected dynamical systems (ePDS). Using this description, in [14] existence and forward completeness (i.e., existence of solutions on $[0, \infty)$) of solutions of ePDS in general and HIGS-controlled systems in particular has been established (in open-loop and closed-loop settings as considered in this paper, for bounded, piecewise constant inputs).

Preprint submitted to Automatica
Received November 20, 2023 08:38:48 Pacific Time

3 Discrete-Time HIGS

In this section, we present two DT versions of HIGS, which preserve the main characteristics and the working principle of CT HIGS elements as in (4). In particular, we present DT variants of HIGS that:

(i) operate as a linear DT integrator as long as the resulting DT trajectories satisfy the sector constraint (5) ;
(ii) switch to other operating regimes only when required to make the sector $\mathcal{S}$, as in (5), forward invariant, i.e., to ensure that the input-output trajectories of DT HIGS satisfy (5) at all discrete times.

For the proposed DT HIGS versions, we will provide formal analysis tools in Sections 4 and 5.

3.1 DT HIGS: A bimodal version

In this section we present a first DT version of HIGS, which is obtained by discretization of the individual operating modes of CT HIGS (4) and is given by

$$\tilde{\mathscr{H}}: \begin{cases} x_h[k] = x_h[k-1] + \omega_h T_s e[k], & \text{if } \xi[k] \in \tilde{\mathscr{F}}_1, \quad (8a) \\ x_h[k] = k_h e[k], & \text{if } \xi[k] \in \tilde{\mathscr{F}}_2, \quad (8b) \\ u[k] = x_h[k], & \quad (8c) \end{cases}$$

where $e[k] \in \mathbb{R}$, $x_h[k] \in \mathbb{R}$, and $u[k] \in \mathbb{R}$ denote the input, state and output of the system, respectively, at time instant $t = kT_s$, with $k \in \mathbb{N}$ the discrete time-step, and $T_s \in \mathbb{R}_{>0}$ the sampling period. The decision of which mode of operation is active is based on the decision variable $\xi[k] := (e[k], u^-[k], e^-[k]) := (e[k], u[k-1], e[k-1])$, while the regions where different subsystems are active, are denoted by $\tilde{\mathscr{F}}_1$, $\tilde{\mathscr{F}}_2 \subseteq \mathbb{R}^3$, which will be specified below.

The DT integrator mode dynamics are given by (8a), obtained by backward Euler discretization of (4a). Moreover, the DT gain mode dynamics are given by (8b). In view of specifications (i) and (ii) above, given an input e, a DT HIGS element should primarily operate in the integrator mode (8a), while generating an output u such that $(e[k], u[k]) \in \mathcal{S}$, for all $k \in \mathbb{N}$, with $\mathcal{S}$ as defined in (5). We assume that $(e[0], u[0]) \in \mathcal{S}$, which, given $e[0]$, can always be arranged by a proper choice of $u[0] = x_h[0]$ (e.g., $u[0] = 0$ is always a viable choice). Thereto, we define

$$\begin{aligned} \tilde{\mathscr{F}}_1 :=& \{\xi = (e, u^-, e^-) \in \mathbb{R}^3 \mid (e^-, u^-) \in \mathcal{S} \\ & \wedge (u^- + \omega_h T_s e)e \geq \frac{1}{k_h}(u^- + \omega_h T_s e)^2\}, \end{aligned} \quad (9)$$

as the region where the integrator mode dynamics (8a) are active. Note that the second condition defining the set in (9) is "testing" if operation according to the integrator mode dynamics (8a), would lead to trajectories that satisfy the sector constraint, as computed in $(u^- + \omega_h T_s e)e \geq \frac{1}{k_h}(u^- + \omega_h T_s e)^2$, in (9). When this is not the case, the gain mode dynamics are active, which leads to the active region

$$\begin{aligned} \tilde{\mathscr{F}}_2 :=& \{\xi = (e, u^-, e^-) \in \mathbb{R}^3 \mid (e^-, u^-) \in \mathcal{S} \\ & \wedge (u^- + \omega_h T_s e)e < \frac{1}{k_h}(u^- + \omega_h T_s e)^2\}, \end{aligned} \quad (10)$$

as it results in operation in the gain mode (8b) only if the trajectories resulting from the integrator mode (8a) would violate (5).

Assumption 1. *The parameters ω_h, k_h, and T_s, are such that $0 < T_s \leq \frac{k_h}{\omega_h}$.*

Assumption 1 can be easily satisfied by design and ensures that (8) always operates in the integrator mode from zero initial conditions. This is an important property, as otherwise, given an input e, a DT HIGS element would only operate in the integrator mode if there has been a sign change in successive input samples. This is clearly undesirable as the integrator mode should be the primary mode of operation of DT HIGS. Indeed for $x_h[k-1] = u[k-1] = 0$, the output of the integrator mode is given by $u[k] = \omega_h T_s e[k]$, which under Assumption 1 satisfies $(e[k], u[k]) \in \mathcal{S}$.

An illustration of the regions $\tilde{\mathscr{F}}_1$, and $\tilde{\mathscr{F}}_2$, when $k_h = \omega_h = 1$, $T_s = 0.5$, is provided in Fig. 1. Note that while

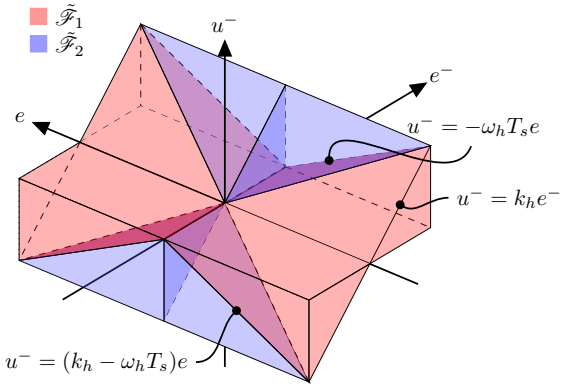

Fig. 1. Regions $\tilde{\mathscr{F}}_1$, and $\tilde{\mathscr{F}}_2$, in the (e, u^-, e^-) space.

the gain mode dynamics (4b) of a CT HIGS element are active on a subset of a lower-dimensional subspace of the $(e, u, \dot{e})$ space (see Fig. 3 in [6]) and thus in a region with empty interior (due to the condition $u = k_h e$ in (6)), as shown in Fig. 1, both modes of (8) are active on sets with non-empty interiors.

3.2 DT HIGS: A trimodal version

In this section, we present an alternative DT HIGS which ensures forward invariance of the sector $\mathcal{S}$ by means of

Preprint submitted to Automatica
Received November 20, 2023 08:38:48 Pacific Time

projecting the integrator dynamics in (8a) onto the sector. In view of specification (i) (see the beginning of Section 3), we define the primary mode of operation of DT HIGS as

$$\begin{aligned} x_h[k] = u_{int}[k] &:= x_h[k-1] + \omega_h T_s e[k], \\ u[k] &= x_h[k], \end{aligned} \tag{11}$$

which is similar to the integrator-mode dynamics (8a), of the bimodal DT HIGS. As in the case of (8), we assume $(e[0], u[0]) \in \mathcal{S}$. Moreover, it is also assumed that Assumption 1 holds, as it ensures that for zero initial conditions, the integrator dynamics always produce trajectories that belong to $\mathcal{S}$.

In order to have forward invariance of $\mathcal{S}$, we project the integrator dynamics along u onto $\mathcal{S}$, leading to

$$x_h[k] = \begin{cases} P_{[0,k_h e[k]]}(u_{int}[k]), & \text{if } e[k] \geq 0, \quad (12a) \\ P_{[k_h e[k],0]}(u_{int}[k]), & \text{if } e[k] \leq 0, \quad (12b) \end{cases}$$

with $u_{int}[k]$ as defined in (11) and $P_{\mathcal{I}}(v) := \text{argmin}_{a \in \mathcal{I}} |a - v|$, for a set $\mathcal{I} \subseteq \mathbb{R}$. Note that (12) is inspired by the re-written expression of $\mathcal{S}$ as

$$\begin{aligned} \mathcal{S} = &\{(e,u) \in \mathbb{R}^2 \mid e \geq 0 \wedge u \in [0, k_h e]\} \cup \\ &\{(e,u) \in \mathbb{R}^2 \mid e \leq 0 \wedge u \in [k_h e, 0]\}. \end{aligned}$$

It is easy to see (as illustrated in Fig. 2) that for $e[k] \geq 0$

$$P_{[0,k_h e[k]]}(v) = \begin{cases} v, & \text{if } 0 \leq v \leq k_h e[k], \\ k_h e[k], & \text{if } v \geq k_h e[k], \\ 0, & \text{if } v \leq 0, \end{cases} \tag{13}$$

and similar expressions hold for $e[k] \leq 0$, i.e.,

$$P_{[k_h e[k],0]}(v) = \begin{cases} v, & \text{if } k_h e[k] \leq v \leq 0, \\ k_h e[k], & \text{if } v \leq k_h e[k], \\ 0, & \text{if } v \geq 0. \end{cases} \tag{14}$$

Note that by using a similar reasoning as in Section 3.1, when $\xi[k] := (e[k], u^-[k], e^-[k]) := (e[k], u[k-1], e[k-1]) \in \tilde{\mathscr{F}}_1$, with $\tilde{\mathscr{F}}_1$ as defined in (9), one has $0 \leq |u_{int}[k]| \leq k_h |e[k]|$ and therefore, by solving (12) the integrator dynamics (11) are obtained. Next, let us consider the case where $\xi[k] \in \tilde{\mathscr{F}}_2$ with $\tilde{\mathscr{F}}_2$ as defined in (10). For $e[k] \geq 0$ and $e[k]^- e[k] \geq 0$ (and thus $e^-[k] \geq 0$), we have $x_h[k-1] = u^-[k] \geq 0$ (since $(e^-[k], u^-[k]) \in \mathcal{S}$) which in turn results in $x_h[k-1] + \omega_h T_s e[k] \geq 0$. As a result, $\xi[k] \in \tilde{\mathscr{F}}_2$ and $e^-[k] e[k] \geq 0$, implies $u_{int}[k] > k_h e[k]$, leading to $P_{[0,k_h e[k]]}(u_{int}[k]) = k_h e[k]$. Similar arguments can be used for $e[k] \leq 0$ to show that if $\xi[k] \in \tilde{\mathscr{F}}_2$ and $e^-[k] e[k] \geq 0$, then $P_{[k_h e[k],0]}(u_{int}[k]) = k_h e[k]$.

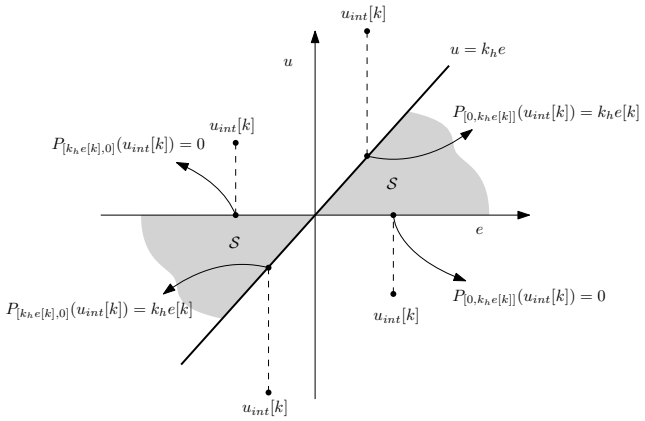

Fig. 2. input-output (e,u)-plane of DT HIGS and possible outcomes of projection.

Therefore, solving (12) leads to $x_h[k] = k_h e[k]$, when $\xi[k] \in \overline{\mathscr{F}}_2$, with

$$\overline{\mathscr{F}}_2 := \{\xi = (e, u^-, e^-) \in \mathbb{R}^3 \mid \xi \in \tilde{\mathscr{F}}_2 \wedge e e^- \geq 0\}. \tag{15}$$

Moreover when $\xi[k] \in \tilde{\mathscr{F}}_2$, for $e[k] \geq 0$ and $e^-[k] e[k] \leq 0$ we have $x_h[k-1] = u^-[k] \leq 0$ (since $(e^-, u^-) \in \mathcal{S}$). As a result of Assumption 1 we have $x_h[k-1] + \omega_h T_s e[k] \leq k_h e[k]$. Therefore $\xi[k] \in \tilde{\mathscr{F}}_2$ implies $u_{int}[k] < 0$ and thus $P_{[0,k_h e[k]]}(u_{int}[k]) = 0$. By using similar arguments for the case where $e[k] \leq 0$ we conclude that solving (12) leads to $x_h[k] = 0$ when $\xi[k] \in \overline{\mathscr{F}}_3$, with

$$\overline{\mathscr{F}}_3 := \{\xi = (e, u^-, e^-) \in \mathbb{R}^3 \mid \xi \in \tilde{\mathscr{F}}_2 \wedge e e^- < 0\}. \tag{16}$$

As a result of the discussions above, solving (12), leads us to the explicit piecewise linear system representation

$$\overline{\mathscr{H}} : \begin{cases} x_h[k] = x_h[k-1] + \omega_h T_s e[k], & \text{if } \xi[k] \in \overline{\mathscr{F}}_1, \quad (17a) \\ x_h[k] = k_h e[k], & \text{if } \xi[k] \in \overline{\mathscr{F}}_2, \quad (17b) \\ x_h[k] = 0, & \text{if } \xi[k] \in \overline{\mathscr{F}}_3, \quad (17c) \\ u[k] = x_h[k], & \quad (17d) \end{cases}$$

of the so-called trimodal DT HIGS. An illustration of the regions $\overline{\mathscr{F}}_1$, $\overline{\mathscr{F}}_2$, and $\overline{\mathscr{F}}_3$, when $k_h = \omega_h = 1$, $T_s = 0.5s$, is provided in Fig. 3.

The response of a CT HIGS element (4) to a sinusoidal input, is compared to those of DT HIGS elements as in (8) and (17) in Fig. 4. As it can be seen in Fig. 4, initially the three responses are similar to each other. After a zero crossing in the input e, however, the trimodal DT HIGS (17) element generates an output, which is much closer to the output of the CT HIGS (4) element, for finite positive values of T_s. In the next two sections we will present tools to analyze these two DT versions in closed-loop settings.

Preprint submitted to Automatica
Received November 20, 2023 08:38:48 Pacific Time

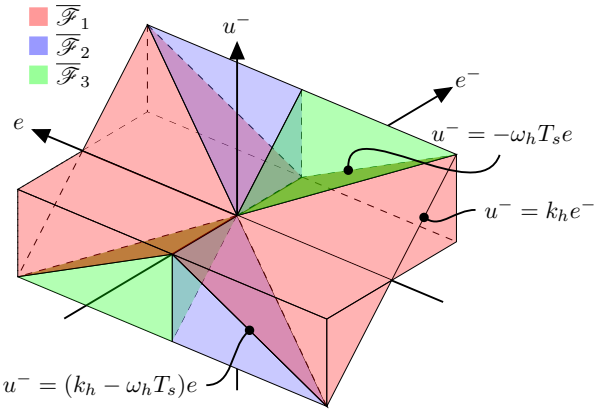

Fig. 3. Regions $\overline{\mathscr{F}}_1$, $\overline{\mathscr{F}}_2$, and $\overline{\mathscr{F}}_3$ in the (e, u^-, e^-) space.

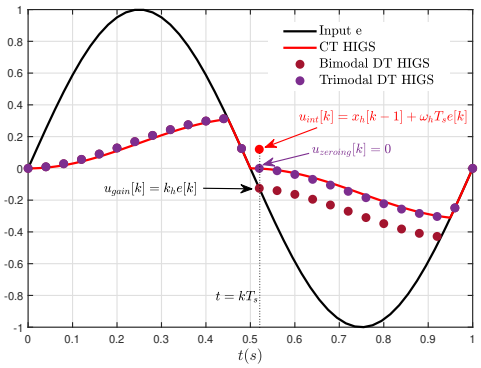

Fig. 4. Response of CT and the different DT HIGS elements with $k_h = \omega_h = 1$, $T_s = 0.04s$, to a sinusoidal input.

4 Stability analysis of DT HIGS-controlled systems

In this section we present stability conditions for DT HIGS-controlled systems. In particular, conditions are presented that can be used to certify ISS of DT HIGS-controlled systems based on both (measured) frequency response functions (Section 4.2) and LMIs (Section 4.3). The relation between the two criteria will be discussed in Section 4.4.

4.1 DT Closed-loop system description

We consider the closed-loop system in Fig. 5, consisting of a DT LTI system $\overline{\mathscr{G}}$ and a DT HIGS element $\mathcal{H}_{DT}$, which can be one of the two versions discussed in the previous section. Here, $\overline{\mathscr{G}}$ contains the linear part of the loop, consisting of the plant to be controlled and possibly LTI parts of the controller. The system $\overline{\mathscr{G}}$ is given by

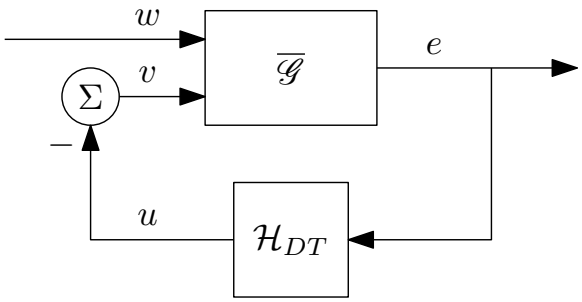

Fig. 5. DT HIGS-controlled closed-loop system.

$$\overline{\mathscr{G}}: \begin{cases} x_g[k] &= A_g x_g[k-1] + B_{gv} v[k-1] + B_{gw} w[k-1], \\ e[k] &= C_g x_g[k] \end{cases} \tag{18}$$

with state $x_g[k]$ taking values in $\mathbb{R}^{n_g}$, output $e[k]$ taking values in $\mathbb{R}$, control input $v[k]$ in $\mathbb{R}$ and exogenous disturbances $w[k]$ in $\mathbb{R}^{n_w}$, at discrete time $k \in \mathbb{N}$. Moreover, A_g, B_{gv}, B_{gw}, and C_g are real matrices of appropriate dimensions. The DT HIGS element $\mathcal{H}_{DT}$ is given by either (8) or (17). For the closed-loop interconnection in Fig. 5, we have the state $x[k] = [x_g^\top[k]\ x_h^\top[k]]^\top \in \mathbb{R}^n$, where $n = n_g + 1$. In the case where $\mathcal{H}_{DT}$ is given by (8), by combining (8) and (18), we arrive at the state-space representation

$$\Sigma: \begin{cases} x[k] = A_i x[k-1] + B_i w[k-1], \ \text{if } \xi[k] \in \tilde{\mathscr{F}}_i, i \in \{1,2\} \\ e[k] = Cx[k], \end{cases} \tag{19}$$

for the closed-loop dynamics with $\tilde{\mathscr{F}}_i$, $i \in \{1,2\}$, as defined in (9) and (10), and

$$[\,A_1 \,|\, B_1\,] = \left[\begin{array}{cc|c} A_g & -B_{gv} & B_{gw} \\ \omega_h T_s C_g A_g & 1 - \omega_h T_s C_g B_{gv} & \omega_h T_s C_g B_{gw} \end{array}\right], \tag{20}$$

$$[\,A_2 \,|\, B_2\,] = \left[\begin{array}{cc|c} A_g & -B_{gv} & B_{gw} \\ k_h C_g A_g & -k_h C_g B_{gv} & k_h C_g B_{gw} \end{array}\right], \tag{21}$$

$$C = [\,C_g \ 0\,]. \tag{22}$$

In the case where the HIGS element $\mathcal{H}_{DT}$ is given by (17), we obtain

$$\Sigma: \begin{cases} x[k] = A_i x[k-1] + B_i w[k-1], \text{if } \xi[k] \in \overline{\mathscr{F}}_i, i \in \{1,2,3\} \\ e[k] = Cx[k], \end{cases} \tag{23}$$

with $\overline{\mathscr{F}}_i$, $i \in \{1,2,3\}$, as defined in (9), (15), and (16), the matrices A_i, B_i, C, $i \in \{1,2\}$ as defined in (20), (21),

Preprint submitted to Automatica
Received November 20, 2023 08:38:48 Pacific Time

(22), and

$$\left[\begin{array}{c|c} A_3 & B_3 \end{array}\right] = \left[\begin{array}{cc|c} A_g & -B_{gv} & B_{gw} \\ 0 & 0 & 0_{1\times n_w} \end{array}\right]. \tag{24}$$

In the next subsections, we study ISS of (19) and (23) as in Definition 2.

4.2 Frequency-domain stability conditions

In this section results are presented, which guarantee ISS of (19) and (23), using simple-to-check graphical conditions based on frequency response functions. As accurate frequency response functions can generally be measured quickly in practice (e.g., in mechatronic positioning systems), and provide a model dedicated to the system under consideration, such frequency-based conditions for ISS, are appealing to control practitioners.

Theorem 2. *Consider systems* (19) *and* (23) *with* (A_g, B_{gv}, C_g) *being a minimal realization. The systems are ISS, if*

i) The system matrix A_g *is Schur;*
ii) $\frac{1}{k_h} + Re\{W(z)\} > 0$, *for all* $z \in \mathbb{C}$, $|z| = 1$, *with*

$$W(z) = C_g(zI - A_g)^{-1}B_{gv}. \tag{25}$$

Proof. The proof is based on showing that under the conditions stated in the theorem, there exists an ISS Lyapunov function for the systems under consideration, which by Theorem 1 implies ISS of the underlying systems. The proof is divided into the following steps:

(i) Initially we use stability of $\overline{\mathscr{G}}$, implied by i), positive realness of $C_g(zI - A_g)^{-1}B_{gv} + \frac{1}{k_h}$, following from ii), minimality of (A_g, B_{gv}, C_g), and the fact that $u[k]e[k] \geq \frac{1}{k_h}u^2[k]$ for all $k \in \mathbb{N}$, to construct a quadratic ISS Lyapunov function $V_g(x_g) = x_g^\top P_g x_g$, with $P_g \succ 0$ for $\overline{\mathscr{G}}$, by application of the DT KYP Lemma [3, 24].
(ii) For both cases where $\mathcal{H}_{DT}$ is given by (8) or (17), a quadratic Lyapunov-like function $V_h(x_h)$ is constructed for the DT HIGS $\mathcal{H}_{DT}$ in isolation with input $e[k-1] = C_g x_g[k-1]$. By explicit use of the sector constraint of $\mathcal{H}_{DT}$ it is shown that the Lyapunov function decreases along the trajectories of the DT-HIGS element.
(iii) The functions V_g and V_h constructed in the previous steps are combined into a single quadratic ISS Lyapunov function for the underlying closed-loop systems, thereby proving the theorem.

Throughout the proof we have dropped time dependence, where clear from the context, to lighten the notation.
Step 1: It follows from the DT KYP Lemma [3] (sometimes also referred to as the Kalman-Szegö-Popov Lemma), that the minimality of (A_g, B_{gv}, C_g), together with the hypotheses in the Theorem imply the existence of a symmetric positive definite matrix P_g, a matrix L and a positive constant ε such that

$$\begin{aligned} A_g^\top P_g A_g - P_g &= -L^\top L - \varepsilon P_g, \\ B_{gv}^\top P_g A_g &= C_g - \sqrt{\frac{2}{k_h} - B_{gv}^\top P_g B_{gv}}\ \ L. \end{aligned} \tag{26}$$

Consider the Lyapunov function $V_g(x_g) = x_g^\top P_g x_g$. One has

$$\begin{aligned} &\Delta V_g := V_g(A_g x_g + B_{gv}v + B_{gw}w) - V_g(x_g) \\ &= (A_g x_g + B_{gv}v + B_{gw}w)^\top P_g (A_g x_g + B_{gv}v + B_{gw}w) \\ &- x_g^\top P_g x_g = x_g^\top (A_g^\top P_g A_g - P_g) x_g + \\ &2x_g^\top A_g^\top P_g B_{gv} v + 2x_g^\top A_g^\top P_g B_{gw} w + \\ &v^\top B_{gv}^\top P_g B_{gv} v + 2v^\top B_{gv}^\top P_g B_{gw} w + w^\top B_{gw}^\top P_g B_{gw} w. \end{aligned}$$

Using (26) and $v = -x_h$, yields

$$\begin{aligned} &\Delta V_g = x_g^\top (-L^\top L - \varepsilon P_g) x_g \\ &- 2x_g^\top (C_g^\top - \sqrt{\frac{2}{k_h} - B_{gv}^\top P_g B_{gv}}\ \ L^\top) x_h \\ &+ 2x_g^\top A_g^\top P_g B_{gw} w + x_h^\top B_{gv}^\top P_g B_{gv} x_h - 2x_h^\top B_{gv}^\top P_g B_{gw} w \\ &+ w^\top B_{gw}^\top P_g B_{gw} w \end{aligned}$$

by using the sector constraint (5) of $\mathcal{H}_{DT}$ and reworking the expression above we get

$$\begin{aligned} &\Delta V_g \leq -\varepsilon V_g(x_g) - \tilde{L}^\top \tilde{L} \\ &+ \left(2x_g^\top A_g^\top P_g B_{gw} - 2x_h^\top B_{gv}^\top P_g B_{gw} + w^\top B_{gw}^\top P_g B_{gw}\right) w \\ &\leq -\varepsilon V_g(x_g) + \\ &\left(2x_g^\top A_g^\top P_g B_{gw} - 2x_h^\top B_{gv}^\top P_g B_{gw} + w^\top B_{gw}^\top P_g B_{gw}\right) w, \end{aligned}$$

with $\tilde{L} = \left(Lx_g - \sqrt{\frac{2}{k_h} - B_{gv}^\top P_g B_{gv}}\ x_h\right)$. Moreover, note that

$$\begin{aligned} &\left(2x_g^\top A_g^\top P_g B_{gw} - 2x_h^\top B_{gv}^\top P_g B_{gw} + w^\top B_{gw}^\top P_g B_{gw}\right) w \\ &\leq 2\lambda_{\max}(P_g)\|A_g\|\|B_{gw}\|\|x_g\|\|w\| + \\ &2\lambda_{\max}(P_g)\|B_{gv}\|\|B_{gw}\|\|x_h\|\|w\| + \lambda_{\max}(P_g)\|B_{gw}\|^2\|w\|^2 \\ &\leq \alpha_1\|x_g\|\|w\| + \alpha_2\|x_g\|\|w\| + \alpha_3\|w\|^2 = \alpha_4\|x_g\|\|w\| + \\ &\alpha_3\|w\|^2, \end{aligned}$$

with $\alpha_1 = 2\lambda_{\max}(P_g)\|A_g\|\|B_{gw}\|$, $\alpha_3 = \lambda_{\max}(P_g)\|B_{gw}\|^2$, $\alpha_2 = 2\lambda_{\max}(P_g)k_h\|B_{gv}\|\|B_{gw}\|\|C_g\|$, $\alpha_4 = \alpha_1 + \alpha_2$, and where we have used that $\|x_h\| \leq k_h\|C_g\|\|x_g\|$. Note that the latter is a direct consequence of the sector condition (5). Indeed, as a result of (5) the input and output of

Preprint submitted to Automatica
Received November 20, 2023 08:38:48 Pacific Time

the HIGS element satisfy $\|x_h\| = \|u_h\| \leq k_h\|e\|$. Noting that $e = C_g x_g$, we conclude $\|x_h\| \leq k_h\|C_g\|\|x_g\|$. By using Young's inequality, we get

$$\Delta V_g \leq -\underbrace{\left(\varepsilon\lambda_{\min}(P_g) - \frac{\alpha_4}{2\delta_1}\right)}_{c_1}\|x_g\|^2 + \underbrace{\left(\frac{\alpha_4\delta_1}{2} + \alpha_3\right)}_{c_2}\|w\|^2. \tag{27}$$

Note that both c_1 and c_2 are both positive, if δ_1 is taken sufficiently large.

Step 2: Consider the quadratic Lyapunov function $V_h(x_h) = x_h^2$, for the isolated DT HIGS element $\mathcal{H}_{DT}$, given by (8) or (17). When $\mathcal{H}_{DT}$ operates in the integrator mode, i.e., according to (8a) or (17a), we have

$$\begin{aligned}
&\Delta V_h(x_h[k]) := V_h(x_h[k]) - V_h(x_h[k-1]) = \\
&\Delta V_{h,\text{int}}(x_h[k-1]) := V_h(x_h[k-1] + \omega_h T_s e[k]) - V_h(x_h[k-1]) \\
&= (x_h[k-1] + \omega_h T_s e[k])^2 - x_h^2[k-1] = 2\omega_h T_s e[k] x_h[k-1] \\
&+ (\omega_h T_s)^2 e^2[k] \\
&\leq \omega_h T_s x_h^2[k-1] + (\omega_h T_s + (\omega_h T_s)^2) e^2[k] = -c_3 x_h^2[k-1] \\
&+ (c_3 + \omega_h T_s) x_h^2[k-1] + (\omega_h T_s + (\omega_h T_s)^2) e^2[k]
\end{aligned} \tag{28}$$

for some $c_3 > 0$, and where we have made use of Young's inequality. Once again using the sector constraint (5) of $\mathcal{H}_{DT}$ and applying Young's inequality for products yields

$$\begin{aligned}
&\Delta V_{h,\text{int}}(x_h[k-1]) \leq -c_3\|x_h^2[k-1]\| + \\
&(c_3 k_h + \omega_h T_s k_h)\|C_g\|^2\|x_g[k-1]\|^2 \\
&+ \underbrace{(\omega_h T_s + (\omega_h T_s)^2)}_{\tilde{\alpha}}\|e[k]\|^2.
\end{aligned}$$

Note that by using (18) and application of Young's inequality we get

$$\|e[k]\|^2 \leq (\tilde{\alpha}_1 + \tilde{\alpha}_2(k_h\|C_g\|^2)\|x_g[k-1]\|^2 + \tilde{\alpha}_3\|w[k-1]\|^2, \tag{29}$$

with

$$\begin{aligned}
\tilde{\alpha}_1 &= \|C_g A_g\|^2 + \|C_g A_g\|\|C_g B_{gv}\| + \|C_g A_g\|\|C_g B_{gw}\|, \\
\tilde{\alpha}_2 &= \|C_g A_g\|\|C_g B_{gv}\| + \|C_g B_{gv}\|^2 + \|C_g A_g\|\|C_g B_{gw}\|, \\
\tilde{\alpha}_3 &= \|C_g A_g\|\|C_g B_{gw}\| + \|C_g B_{gw}\|^2 + \|C_g A_g\|\|C_g B_{gv}\|.
\end{aligned}$$

Therefore, we have

$$\begin{aligned}
&\Delta V_{h,\text{int}}(x_h) \leq -c_3\|x_h\|^2 \\
&+ \underbrace{\left((c_3 k_h + \omega_h T_s k_h)\|C_g\|^2 + \tilde{\alpha}\tilde{\alpha}_1 + \tilde{\alpha}\tilde{\alpha}_2 k_h\|C_g\|^2\right)}_{\beta_1}\|x_g\|^2 \\
&+ \underbrace{\tilde{\alpha}\tilde{\alpha}_3}_{\gamma_1}\|w\|^2,
\end{aligned}$$

where we have dropped the time arguments for ease of notation.

When $\mathcal{H}_{DT}$ operates in the gain mode, i.e., either according to (8b) or (17b), we have

$$\begin{aligned}
&\Delta V_h(x_h[k]) := V_h(x_h[k]) - V_h(x_h[k-1]) = \\
&\Delta V_{h,\text{gain}}(x_h[k-1]) := x_h^2[k] - x_h^2[k-1] = k_h^2 e^2[k] - x_h^2[k-1] \\
&\leq -x_h[k-1]^2 + k_h^2\tilde{\alpha}_1\|x_g[k-1]\|^2 \\
&+ k_h^2\tilde{\alpha}_2 k_h^2\|C_g\|^2\|x_g[k-1]\|^2 + k_h^2\tilde{\alpha}_3\|w\|^2
\end{aligned}$$

with $\tilde{\alpha}_i$, $i \in \{1,2,3\}$, as defined above. As such, we get

$$\begin{aligned}
&\Delta V_{h,\text{gain}}(x_h) \leq \\
&-x_h^2 + \underbrace{(k_h^2\tilde{\alpha}_1 + k_h^4\tilde{\alpha}_2\|C_g\|^2)}_{\beta_2}\|x_g\|^2 + \underbrace{k_h^2\tilde{\alpha}_3}_{\gamma_2}\|w\|^2.
\end{aligned} \tag{30}$$

Lastly, when $\mathcal{H}_{DT}$ is given by (17), and it operates in the zeroing mode (17c), we have

$$\begin{aligned}
&\Delta V_h(x_h[k]) := V_h(x_h[k]) - V_h(x_h[k-1]) = \\
&\Delta V_{h,\text{zero}}(x_h[k-1]) := V(0) - V(x_h[k-1]) = -x_h^2[k-1].
\end{aligned} \tag{31}$$

Hence, for both cases wherein $\mathcal{H}_{DT}$ is given by (8) or (17), one has

$$\Delta V_h(x_h) \leq -\overline{\alpha}\|x_h\|^2 + \overline{\beta}\|x_g\|^2 + \overline{\gamma}\|w\|^2, \tag{32}$$

along all modes of operation, with $\overline{\alpha} = \min(1, c_3)$, $\overline{\beta} = \max(\beta_1, \beta_2)$, and $\overline{\gamma} = \max(\gamma_1, \gamma_2)$.

Step 3: Let us now consider the closed-loop system in Fig. 5. Consider the Lyapunov function

$$V(x_g, x_h) = V_g(x_g) + \mu V_h(x_h) = x^\top P x,$$

with $x = \begin{bmatrix} x_g^\top & x_h^\top \end{bmatrix}^\top$, $P = \begin{bmatrix} P_g & 0 \\ 0 & \mu \end{bmatrix}$, and some $\mu > 0$. Note that $P \succ 0$ due to P_g being positive define and $\mu > 0$. As a result of (27) and (32), for the closed-loop system (19) and (23), the one-step difference in the Lyapunov function $V(x_g, x_h)$, given by $\Delta V(x) := V(A_i x + B_i w) - V(x)$, with $i \in \{1,2\}$ for $\mathcal{H}_{DT}$ as in (8a) and $i \in \{1,2,3\}$ for $\mathcal{H}_{DT}$ as in (17a), satisfies

$$\begin{aligned}
&\Delta V(x) = \Delta V_g + \mu\Delta V_h \\
&\leq -(c_1 - \mu\overline{\beta})\|x_g\|^2 - \mu\overline{\alpha}\|x_h\|^2 + (c_2 + \mu\overline{\gamma})\|w\|^2 \\
&\leq -\kappa_1\|x\|^2 + \kappa_2\|w\|^2,
\end{aligned} \tag{33}$$

with $\kappa_1 := \min\left((c_1 - \mu\overline{\beta}), \mu\overline{\alpha}\right)$, $\kappa_2 := c_2 + \mu\overline{\gamma}$, and μ sufficiently small such that $c_1 - \mu\overline{\beta} > 0$. This shows that $V(x_g, x_h)$ is an ISS Lyapunov function for both (19) and (23), thereby concluding the proof. □

Preprint submitted to Automatica
Received November 20, 2023 08:38:48 Pacific Time

The conditions in Theorem 2 resemble the Tsypkin criterion [18], which is the DT analog of the CT circle criterion [17] for the study of DT absolute stability. However, while the Tsypkin criterion is concerned with memoryless nonlinearities, DT HIGS is a dynamical system with memory, thereby requiring additional steps and arguments in the proof (particularly step 2 and its integration with step 1 in step 3). Theorem 2 can be verified using easy-to-measure frequency response functions (FRFs). In particular, condition i) can be checked using standard linear control arguments. For a given value of $k_h \in \mathbb{R}_{>0}$, checking condition ii), boils down to checking whether the Nyquist plot of $W(e^{j\omega})$ lies to the right of the vertical line passing through the point $\frac{-1}{k_h}+j0$ in the complex plane, for all $\omega \in [0, 2\pi]$.

4.3 Time-domain stability analysis

In this section we present LMI-based conditions that guarantee ISS of (19) and (23) using a multiple Lyapunov function approach [7]. In doing so, we exploit the fact that the input-output pairs of the proposed DT HIGS elements (8) and (17) belong to the set $\mathcal{S}$ on (5), for all $k \in \mathbb{N}$. In particular, we partition the input-output space of the DT HIGS element $\mathcal{H}_{DT}$ and allow different Lyapunov functions to be active within each region of the partition. The partitioning employed in this work is similar to the one used in [19, 32, 34] for reset control systems and CT HIGS-controlled systems, but is now extended towards a DT setting. More specifically, the input-output $e-u$ plane is partitioned into N sub-sectors $\mathscr{C}_i$, $i \in \{1, 2, \dots, N\}$, by choosing $N+1$ equidistantly spaced angles $0 = \theta_0 < \theta_1 < \cdots < \theta_N = \arctan(k_h)$ (see Fig. 3 in [25]). Loosely speaking, $\mathscr{C}_i$ is related to the sector $[\theta_{i-1}, \theta_i]$ in the $e-u$ plane. As shown in [32, 34], for every pair (e, u) located in $\mathscr{C}_i$ one has

$$\underbrace{\begin{bmatrix} -\sin\theta_{i-1} & \cos\theta_{i-1} \\ \sin\theta_i & -\cos\theta_i \end{bmatrix}}_{E_i} \begin{bmatrix} e \\ u \end{bmatrix} \geq 0 \tag{34}$$

for all (e, u) in the first quadrant of the $e-u$ plane, and $E_i \begin{bmatrix} e \\ u \end{bmatrix} \leq 0$, for all (e, u) in the third quadrant of the $e-u$ plane. Moreover, note that the state of the closed-loop system in Fig. 5, can be mapped to the input-output pair of $\mathcal{H}_{DT}$ according to

$$\begin{bmatrix} e[k] \\ u[k] \end{bmatrix} = \underbrace{\begin{bmatrix} C_g & 0 \\ 0 & 1 \end{bmatrix}}_{\overline{C}} \begin{bmatrix} x_g[k] \\ x_h[k] \end{bmatrix}. \tag{35}$$

Therefore, $(e, u) \in \mathscr{C}_i$, $i \in \{1, 2, \dots, N\}$, translates on the level of states to $x \in \mathcal{S}_i$, $i \in \{1, 2, \dots, N\}$, with

$$\mathcal{S}_i = \{x \in \mathbb{R}^n \mid E_i \overline{C} x \geq 0 \vee E_i \overline{C} x \leq 0\} \tag{36}$$

with E_i and $\overline{C}$ defined as in (34) and (35), respectively.

We are now ready to state the main results of this section.

Theorem 3. *Consider the system* (19). *Suppose there exist symmetric matrices* $W_i, U_{1,ij}, U_{2,i}, Y_{1,ij}, Y_{2,i} \in \mathbb{S}^{2\times 2}_{\geq 0}$ *and* $P_i \in \mathbb{S}^{n\times n}$ *, for* $i, j \in \{1, 2, \dots, N\}$, *such that*

$$P_i - \overline{C}^\top E_i^\top W_i E_i \overline{C} \succ 0, \tag{37}$$

$$A_1^\top (P_j + \overline{C}^\top E_j^\top Y_{1,ij} E_j \overline{C}) A_1 - P_i + \overline{C}^\top E_i^\top U_{1,ij} E_i \overline{C} \prec 0, \tag{38}$$

$$A_2^\top (P_N + \overline{C}^\top E_N^\top Y_{2,i} E_N \overline{C}) A_2 - P_i + \overline{C}^\top E_i^\top U_{2,i} E_i \overline{C} \prec 0. \tag{39}$$

Then the closed-loop system (19) *is ISS.*

Proof. Due to (36) together with the non-negativity of the elements in W_i, (37) implies that $V(x) = x^\top P_i x > 0$, when $x \in \mathcal{S}_i$, $i \in \{1, 2, \dots, N\}$ and $x \neq 0$, ensuring positive definiteness of V. Furthermore, in integrator mode, one has

$$\begin{aligned} &\Delta V_1^{ij} := V(A_1 x + B_1 w) - V(x) = \\ &x^\top (A_1^\top P_j A_1 - P_i) x + 2 x^\top A_1^\top P_j B_1 w + w^\top B_1^\top P_j B_1 w, \end{aligned} \tag{40}$$

$i, j \in \{1, \dots, N\}$, when $x \in \mathcal{S}_i$ and $A_1 x + B_1 w \in \mathcal{S}_j$. Note that when $x \in \mathcal{S}_i$ it holds that $x^\top \overline{C}^\top E_i^\top U_{1,ij} E_i \overline{C} x \geq 0$ for $U_{1,ij} \in \mathbb{S}^{2\times 2}_{\geq 0}$, and when $A_1 x + B_1 w \in \mathcal{S}_j$, it holds that

$$\begin{aligned} 0 \leq &(A_1 x + B_1 w)^\top \overline{C}^\top E_j^\top Y_{1,ij} E_j \overline{C} (A_1 x + B_1 w) = \\ &x^\top A_1^\top \overline{C}^\top E_j^\top Y_{1,ij} E_j \overline{C} A_1 x + 2 x^\top A_1^\top \overline{C}^\top E_j^\top Y_{1,ij} E_j \overline{C} B_1 w \\ &+ w^\top B_1^\top \overline{C}^\top E_j^\top Y_{1,ij} E_j \overline{C} B_1 w, \end{aligned} \tag{41}$$

and thus

$$\begin{aligned} &- x^\top A_1^\top \overline{C}^\top E_j^\top Y_{1,ij} E_j \overline{C} A_1 x \leq \\ &2 x^\top A_1^\top \overline{C}^\top E_j^\top Y_{1,ij} E_j \overline{C} B_1 w + w^\top B_1^\top \overline{C}^\top E_j^\top Y_{1,ij} E_j \overline{C} B_1 w \end{aligned} \tag{42}$$

for $Y_{1,ij} \in \mathbb{S}^{2\times 2}_{\geq 0}$. Due to (38), (40), (42) as well as non-negativity of the elements of $Y_{1,ij}$, and $U_{1,ij}$, by application of S-procedure relaxations , we obtain for $x \in \mathcal{S}_i$, $A_1 x + B_1 w \in \mathcal{S}_j$,

$$\begin{aligned} \Delta V_1^{ij} \leq &-\epsilon_1 \|x\|^2 \\ &+ 2 x^\top (A_1^\top P_j B_1 + A_1^\top \overline{C}^\top E_j^\top Y_{1,ij} E_j \overline{C} B_1) w \\ &+ w^\top (B_1^\top P_j B_1 + B_1^\top \overline{C}^\top E_j^\top Y_{1,ij} E_j \overline{C} B_1) w, \end{aligned} \tag{43}$$

Preprint submitted to Automatica
Received November 20, 2023 08:38:48 Pacific Time

for some $\epsilon_1 > 0$. Young's inequality for products yields now

$$\begin{aligned}\Delta V_1^{ij} \leq (-\epsilon_1 + \frac{1}{\delta_1})\|x\|^2 \\ + (\delta_1\|A_1^\top(P_j + \overline{C}^\top E_j^\top Y_{1,ij} E_j \overline{C})B_1\|^2 \\ + \|B_1^\top(P_j + \overline{C}^\top E_j^\top Y_{1,ij} E_j \overline{C})B_1\|)\|w\|^2\end{aligned} \tag{44}$$

with $\delta_1 > 0$, sufficiently large ($\delta_1 > \frac{1}{\epsilon_1}$, when $x \in \mathcal{S}_i$, and $A_1 x + B_1 w \in \mathcal{S}_j$, $i, j \in \{1, 2, \ldots, N\}$). Next, note that after operating in gain mode, the state x lies within the last sub-sector $\mathcal{S}_N$, i.e., one always has $A_2 x + B_2 w \in \mathcal{S}_N$. Therefore, in the gain mode, one has for $x \in \mathcal{S}_i$

$$\begin{aligned}\Delta V_2^{iN} := V(A_2 x + B_2 w) - V(x) = \\ x^\top(A_2^\top P_N A_2 - P_i)x + 2x^\top A_2^\top P_N B_2 w + w^\top B_2^\top P_N B_2 w,\end{aligned} \tag{45}$$

for $i \in \{1, \ldots, N\}$. As a result of (39), noting that $x \in \mathcal{S}_i$ implies $x^\top \overline{C}^\top E_i^\top U_{2,i} E_i \overline{C} x \geq 0$ for $U_{2,j} \in \mathbb{S}^{2\times 2}_{\geq 0}$, and $A_2 x + B_2 w \in \mathcal{S}_N$ implies $(A_2 x + B_2 w)^\top \overline{C}^\top E_N^\top Y_{2,i} E_N \overline{C}(A_2 x + B_2 w) \geq 0$, for $Y_{2,j} \in \mathbb{S}^{2\times 2}_{\geq 0}$, using similar arguments as in (41)- (43) and by application of S-procedure relaxations and Young's inequality for products we get

$$\begin{aligned}\Delta V_2^{iN} \leq (-\epsilon_2 + \frac{1}{\delta_2})\|x\|^2 \\ + (\delta_2\|A_2^\top(P_N + \overline{C}^\top E_N^\top Y_{2,i} E_N \overline{C})B_2\|^2 \\ + \|B_2^\top(P_N + \overline{C}^\top E_N^\top Y_{2,i} E_N \overline{C})B_2\|)\|w\|^2\end{aligned} \tag{46}$$

for some $\epsilon_2 > 0$ and $\delta_2 > \frac{1}{\epsilon_2}$.

Combining (44) and (46) yields

$$\Delta V := V(A_i x + B_i w) - V(x) \leq -\alpha\|x\|^2 + \sigma\|w\|^2, \tag{47}$$

for $i \in \{1, 2\}$ with $\alpha = \min_j(\epsilon_j - \frac{1}{\delta_j})$, $j \in \{1, 2\}$ and $\sigma = \max(\beta, \gamma)$, where

$$\begin{aligned}\beta = \max_{(i,j)}\{\delta_1\|A_1^\top(P_j + \overline{C}^\top E_j^\top Y_{1,ij} E_j \overline{C})B_1\|^2 \\ + \|B_1^\top(P_j + \overline{C}^\top E_j^\top Y_{1,ij} E_j \overline{C})B_1\|\}\end{aligned}$$

$$\begin{aligned}\gamma = \max_i\{\delta_2\|A_2^\top(P_N + \overline{C}^\top E_N^\top Y_{2,i} E_N \overline{C})B_2\|^2 \\ + \|B_2^\top(P_N + \overline{C}^\top E_N^\top Y_{2,i} E_N \overline{C})B_2\|\}\end{aligned}$$

with $i, j \in \{1, \ldots, N\}$. We thus conclude that V is an ISS Lyapunov function for (19), thereby completing the proof. □

Theorem 3 provides sufficient LMI conditions for certifying ISS of the closed-loop system in Fig. 5, when $\mathcal{H}_{DT}$ is given by the bimodal DT HIGS (8). Next, we provide similar conditions for the case where $\mathcal{H}_{DT}$ is given by the trimodal DT HIGS (17).

Theorem 4. *Consider the system* (23)*. Suppose there exist symmetric matrices* $W_i, U_{1,ij}, U_{2,i}, U_{3,i}, Y_{1,ij}, Y_{2,i}, Y_{3,i} \in \mathbb{S}^{2\times 2}_{\geq 0}$ *with non-negative elements, non-negative scalars* $\tau_{2i}, \tau_{3i} \in \mathbb{R}_{\geq 0}$*, and* $P_i \in \mathbb{S}^{n\times n}$ *, for* $i, j \in \{1, 2, \ldots, N\}$*, such that*

$$P_i - \overline{C}^\top E_i^\top W_i E_i \overline{C} \succ 0, \tag{48}$$

$$A_1^\top(P_j + \overline{C}^\top E_j^\top Y_{1,ij} E_j \overline{C})A_1 - P_i + \overline{C}^\top E_i^\top U_{1,ij} E_i \overline{C} \prec 0, \tag{49}$$

$$\begin{aligned}A_2^\top(P_N + \overline{C}^\top E_N^\top Y_{2,i} E_N \overline{C})A_2 - P_i + \overline{C}^\top E_i^\top U_{2,i} E_i \overline{C} \\ + \tau_{2i} Q \prec 0,\end{aligned} \tag{50}$$

$$\begin{aligned}A_3^\top(P_1 + \overline{C}^\top E_1^\top Y_{3,i} E_1 \overline{C})A_3 - P_i + \overline{C}^\top E_i^\top U_{3,i} E_i \overline{C} \\ - \tau_{3i} Q \prec 0\end{aligned} \tag{51}$$

with $Q = \Xi + \Xi^\top$ *where*

$$\Xi = \begin{bmatrix} C_g^\top C_g A_g & \frac{-1}{2} C_g^\top C_g B_{gv} \\ (\frac{-1}{2} C_g^\top C_g B_{gv})^\top & 0 \end{bmatrix}.$$

Then (23) *is ISS.*

Proof. As in the case of Theorem 3, due to (36) and the non-negativity of the elements in W_i, $i \in \{1, \ldots, N\}$, (48) implies that the Lyapunov function $V(x) = x^\top P_i x > 0$, when $x \in \mathcal{S}_i$, $i \in \{, \ldots, N\}$, and $x \neq 0$, and is thus positive definite within the sector of $\mathcal{H}_{DT}$. Following similar arguments as in the proof of Theorem 3, we get

$$\begin{aligned}\Delta V_1^{ij} := V(A_1 x + B_1 w) - V(x) \\ \leq (-\epsilon_1 + \frac{1}{\delta_1})\|x\|^2 + (\delta_1\|A_1^\top(P_j + \overline{C}^\top E_j^\top Y_{1,ij} E_j \overline{C})B_1\|^2 \\ + \|B_1^\top(P_j + \overline{C}^\top E_j^\top Y_{1,ij} E_j \overline{C})B_1\|)\|w\|^2,\end{aligned} \tag{52}$$

with $\epsilon_1 > 0$ and $\delta_1 > \frac{1}{\epsilon_1}$ such that $\epsilon_1 - \frac{1}{\delta_1}$ is positive. In the gain mode, we have for $x \in \mathcal{S}_i$,

$$\begin{aligned}\Delta V_2^{iN} := V(A_2 x + B_2 w) - V(x) = \\ x^\top(A_2^\top P_N A_2 - P_i)x + 2x^\top A_2^\top P_N B_2 w + w^\top B_2^\top P_N B_2 w,\end{aligned} \tag{53}$$

for $i \in \{1, \ldots, N\}$. Note that according to (15), the gain mode is followed when

$$\begin{aligned}e[k]e[k-1] = \frac{1}{2}x^\top[k-1]Qx[k-1] \\ + x^\top[k-1]\underbrace{\begin{bmatrix} I_{n_g} \\ 0 \end{bmatrix} C_g^\top B_{gw}}_{\overline{S}} w[k-1] \geq 0.\end{aligned} \tag{54}$$

Preprint submitted to Automatica
Received November 20, 2023 08:38:48 Pacific Time

Using (54), and following the same reasoning as in (41)-(43) in the proof of Theorem 3, we obtain

$$\begin{aligned}\Delta V_2^{iN} \leq & -(\epsilon_2 - \frac{1}{\delta_2})\|x\|^2 \\ & + (\delta_2 \|A_2^\top \left(P_N + \overline{C}^\top E_N Y_{2,i} E_N \overline{C}\right) B_2 + \tau_{2,i}\overline{S}\|^2 \\ & + \|B_2^\top P_N B_2 + B_2^\top E_N^\top Y_{2,i} E_N \overline{C} B_2\|)\|w\|^2 \end{aligned} \tag{55}$$

for some $\epsilon_2 > 0$ and $\delta_2 > \frac{1}{\epsilon_2}$ such that $\epsilon_2 - \frac{1}{\delta_2} > 0$.

In the zeroing mode, we have for $x \in \mathcal{S}_i$,

$$\begin{aligned}&\Delta V_3^{i1} := V(A_3 x + B_3 w) - V(x) = \\ &x^\top (A_3^\top P_1 A_3 - P_i) x + 2x^\top A_3^\top P_1 B_3 w + w^\top B_3^\top P_1 B_3 w,\end{aligned} \tag{56}$$

for $i \in \{1, \ldots, N\}$. According to (16), the zeroing mode is followed when

$$\begin{aligned}e[k]e[k-1] = & \frac{1}{2} x^\top[k-1] Q x[k-1] \\ & + x^\top[k-1] \underbrace{\begin{bmatrix} I_{n_g} \\ 0 \end{bmatrix} C_g^\top B_{gw}}_{\overline{S}} w[k-1] < 0.\end{aligned}$$

Using the same reasoning as in (55) we get (also noting that after operation in the zeroing mode $A_3 x + B_3 w \in \mathcal{S}_1$),

$$\begin{aligned}\Delta V_3^{i1} \leq & -(\epsilon_3 - \frac{1}{\delta_3})\|x\|^2 \\ & + (\delta_3 \|A_3^\top \left(P_1 + \overline{C}^\top E_1 Y_{3,i} E_1 \overline{C} - \tau_{3,i}\overline{S}\right) B_3 - \tau_{3,i}\overline{S}\|^2 \\ & + \|B_3^\top P_1 B_3 + B_3^\top E_1^\top Y_{3,i} E_N \overline{C} B_3\|)\|w\|^2,\end{aligned} \tag{57}$$

for some $\epsilon_3 > 0$ and $\delta_3 > \frac{1}{\epsilon_3}$ such that $\epsilon_3 - \frac{1}{\delta_3} > 0$.

Combining (52) and (55) and (57) yields

$$\Delta V := V(A_i x + B_i w) - V(x) \leq -\alpha\|x\|^2 + \sigma\|w\|^2, \tag{58}$$

for $i \in \{1, 2, 3\}$, $\alpha = \min_j(\epsilon_j - \frac{1}{\delta_j})$, $j \in \{1, 2, 3\}$, and $\sigma = \max(\beta, \gamma, \zeta)$ with

$$\begin{aligned}\beta = & \max_{(i,j)}\{\delta_1 \|A_1^\top (P_j + \overline{C}^\top E_j^\top Y_{1,ij} E_j \overline{C}) B_1\|^2 \\ & + \|B_1^\top (P_j + \overline{C}^\top E_j^\top Y_{1,ij} E_j \overline{C}) B_1\|\}\end{aligned}$$

$$\begin{aligned}\gamma = & \max_i\{\delta_2 \|A_2^\top (P_N + \overline{C}^\top E_N^\top Y_{2,i} E_N \overline{C}) B_2 + \tau_{2,i}\overline{S}\|^2 \\ & + \|B_2^\top (P_N + \overline{C}^\top E_N^\top Y_{2,i} E_N \overline{C}) B_2\|\},\end{aligned}$$

$$\begin{aligned}\zeta = & \max_i\{\delta_3 \|A_3^\top (P_1 + \overline{C}^\top E_1^\top Y_{2,1} E_1 \overline{C}) B_3 - \tau_{3,i}\overline{S}\|^2 \\ & + \|B_3^\top (P_1 + \overline{C}^\top E_1^\top Y_{3,i} E_1 \overline{C}) B_3\|\},\end{aligned}$$

where $i, j \in \{1, \ldots, N\}$. We thus conclude that V is an ISS Lyapunov function for (23), thereby completing the proof. □

4.4 The link between the two criteria

Considering the closed-loop system in Fig.5, we have thus far presented two sets of stability results for both (19) and (23). In particular, Theorem 2 presents frequency-domain conditions for certifying ISS (for both (19) and (23)), while Theorem 3 and Theorem 4, provide LMI-based conditions for certifying ISS of (19) (consisting of bimodal DT HIGS) and (23) (consisting of trimodal DT HIGS), respectively. The strength of Theorem 2 lies in the fact that it can be verified based on graphical evaluations of FRF measurements. However, this theorem only makes use of sector boundedness of the input-output pair of the HIGS element $\mathcal{H}_{DT}$ and does not exploit specific knowledge related to its dynamics, making it possibly conservative. Moreover, Theorem 2 concludes stability of the closed-loop system on the basis of the existence of a *common* quadratic Lyapunov function (see Step 3 in the proof of Theorem 2). Theorems 3 and 4, on the other hand, make extensive use of specific knowledge related to the internal HIGS dynamics and conclude stability on the basis of the existence of piecewise quadratic Lyapunov functions. Consequently, Theorems 3 and 4 are expected to produce less conservative results when compared to Theorem 2. Next, we prove this formally by stating results relating the satisfaction of the frequency-domain conditions in Theorem 2 to the feasibility of the LMIs in Theorems 3 and 4.

Theorem 5. *Under minimality of (A_g, B_{gv}, C_g), satisfaction of the conditions in Theorem 2 implies feasibility of the LMIs in Theorem 3 with $N \in \mathbb{N}_{\geq 1}$, $W_i = Y_{1,ij} = Y_{2,i} = 0_{2\times 2}$, $U_{1,ij} = U_{2,i} = U = \frac{1}{\alpha}\begin{bmatrix} 0 & 1 \\ 1 & 0 \end{bmatrix}$, and $P_i = \begin{bmatrix} P_g & 0 \\ 0 & \mu \end{bmatrix}$, $i \in \{1, \ldots, N\}$ where $P_g \in \mathbb{S}^{n_g \times n_g}$ is a positive-definite matrix and $\mu \in \mathbb{R}_{>0}$, $\alpha = \sin(\arctan(k_h))$.*

Proof. As shown in Step 3 of the proof of Theorem 2, this theorem concludes ISS of the closed-loop system on the basis of the existence of a Lyapunov function of the form $V(x) = x^\top P x$ with $P = \begin{bmatrix} P_g & 0 \\ 0 & \mu \end{bmatrix}$, wherein $\mu > 0$ and $P_g \in \mathbb{S}^{n_g \times n_g}$ is a positive definite matrix. Therefore, $P_i = P$ is also positive definite and thus satisfies (37) with $W_i = 0$.

Preprint submitted to Automatica
Received November 20, 2023 08:38:48 Pacific Time

Let us now turn our attention to (38). Note that for $N = 1$, with $P_1 = P$ as defined above and A_1 as defined in (20), we have

$$A_1^\top P_1 A_1 - P_1 = \mathcal{I}_1 + \mu Q_1 \tag{59}$$

with

$$\mathcal{I}_1 = \begin{bmatrix} A_g^\top P_g A_g - P_g & -A_g^\top P_g B_{gv} \\ -B_{gv}^\top P_g A_g & B_{gv}^\top P_g B_{gv} \end{bmatrix},$$
$$Q_1 = \begin{bmatrix} (\omega_h T_s)^2 A_g^\top C_g^\top C_g A_g & \omega_h T_s A_g^\top C_g^\top q_1 \\ \star^\top & q_1 q_1^\top - 1 \end{bmatrix}.$$

where $q_1 = 1 - \omega_h T_s C_g B_{gv}$. Also note that with $N = 1$ and the choice of U as specified above we have

$$\overline{C}^\top E_1^\top U E_1 \overline{C} = \begin{bmatrix} 0 & C_g^\top \\ C_g & \frac{-2}{k_h} \end{bmatrix}.$$

By application of the DT KYP lemma (see (26)), we have

$$\mathcal{I}_1 = \begin{bmatrix} -L^\top L - \varepsilon P_g & \sqrt{\frac{2}{k_h} - B_{gv}^\top P_g B_{gv}} L^\top - C_g^\top \\ \star^\top & B_{gv} P_g B_{gv} \end{bmatrix} \tag{60}$$

for some matrix L and a positive constant ε. Therefore, under the conditions stated in the theorem, (38) is given by

$$\mathcal{I}_1 + \mu Q_1 + \overline{C}^\top E_1^\top U E_1 \overline{C} = \underbrace{\begin{bmatrix} -L^\top L - \varepsilon P_g & \sqrt{\frac{2}{k_h} - B_{gv}^\top P_g B_{gv}} L^\top \\ \sqrt{\frac{2}{k_h} - B_{gv}^\top P_g B_{gv}} L & B_{gv} P_g B_{gv} - \frac{2}{k_h} \end{bmatrix}}_{\overline{\mathcal{I}}} + \mu Q_1. \tag{61}$$

By Schur's lemma, the matrix $\overline{\mathcal{I}}$, is negative definite if and only if

$$-L^\top L - \varepsilon P_g + \frac{\left(\frac{2}{k_h} - B_{gv}^\top P_g B_{gv}\right) L^\top L}{\left(-B_{gv}^\top P_g B_{gv} + \frac{2}{k_h}\right)} = -\varepsilon P_g \prec 0$$

and $-L^\top L - \varepsilon P_g \prec 0$, which indeed holds given that P_g is positive definite, and $\varepsilon > 0$. Consequently, (61) is negative definite for $\mu = m_1 > 0$ sufficiently small. Similar reasoning can be used to rewrite (39) as

$$\overline{\mathcal{I}} + \mu \tilde{Q} \tag{62}$$

with

$$\tilde{Q} = \begin{bmatrix} k_h^2 C_g^\top C_g & -k_h^2 C_g^\top C_g B_{gv} \\ -k_h^2 B_{gv}^\top C_g^\top C_g & k_h^2 B_{gv}^\top C_g^\top C_g B_{gv} \end{bmatrix}.$$

Once again, (62) is negative definite for $\mu = m_2 > 0$, sufficiently small. Therefore, under the conditions stated in the theorem, the LMIs (37)- (39) are satisfied with $\mu = \min(m_1, m_2)$, thereby concluding the proof for $N = 1$. Let us lastly note that due to the satisfaction of the LMIs with $N = 1$ and the choice of P specified above, for $N > 1$, the choice $P_i = P$ satisfies the LMIs as well. This completes the proof. □

Next, we state a similar result, linking Theorems 2 and 4.

Theorem 6. *Under minimality of (A_g, B_{gv}, C_g), satisfaction of the conditions in Theorem 2 implies feasibility of the LMIs in Theorem 3 with $N \in \mathbb{N}_{\geq 1}$, $W_i = Y_{1,ij} = Y_{2,i} = Y_{3,i} = 0_{2\times 2}$, $U_{1,ij} = U_{2,i} = U_{3,i} = U = \frac{1}{\alpha}\begin{bmatrix} 0 & 1 \\ 1 & 0 \end{bmatrix}$, and $P_i = \begin{bmatrix} P_g & 0 \\ 0 & \mu \end{bmatrix}$, $\tau_{2i} = \tau_{3i} = 0$ where $P_g \in \mathbb{S}^{n_g \times n_g}$ is a positive-definite matrix and $\mu \in \mathbb{R}_{>0}$, $\alpha = \sin(\arctan(k_h))$.*

Proof. Satisfaction of the LMIs (48), (49), and (50) follows from the exact same arguments as in the proof of Theorem 5. For the satisfaction of (51), we note that under the conditions stated in the theorem, for $N = 1$, (51) can be written as

$$\overline{\mathcal{I}} + \mu \overline{Q}, \tag{63}$$

with $\overline{\mathcal{I}}$ as defined in (61) and $\overline{Q} = \begin{bmatrix} 0 & 0 \\ 0 & -1 \end{bmatrix}$. Following the same reasoning as in the proof of Theorem 5, we conclude that all the LMIs in Theorem 4 are satisfied for μ sufficiently small, thereby concluding the proof. □

With Theorems 5 and 6, we have shown that satisfaction of the conditions in Theorem 2 implies feasibility of a specific case of the LMIs. Consequently, the frequency-domain conditions in Theorem 2 will never yield less conservative stability guarantees than the ones obtained by the LMIs in Theorems 3 and 4.

5 Sampled-data ISS Guarantees

In the previous section, stability criteria were presented that can be used to guarantee ISS for closed-loop HIGS-controlled systems in DT (ignoring inter-sample behavior). In this section we show that DT ISS, implies ISS of sampled-data HIGS-controlled systems, thus also taking into account the inter-sample behavior, building on ideas in [29].

Consider the interconnection in Fig. 6 consisting of a CT linear plant $\mathscr{P}$, and a general DT nonlinear controller ϕ (e.g., a HIGS-based controller), interconnected via a sampler and a zero-order hold device. Here, the plant is

Preprint submitted to Automatica
Received November 20, 2023 08:38:48 Pacific Time

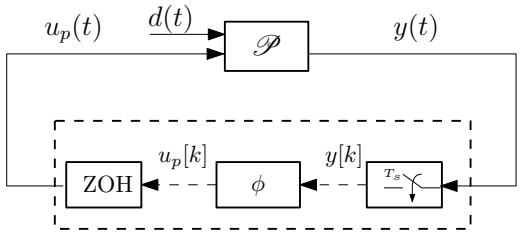

Fig. 6. CT plant $\mathscr{P}$ and sampled-data nonlinear controller.

given by

$$\mathscr{P}: \begin{cases} \dot{x}_p(t) = \mathcal{A}_p x_p(t) + \mathcal{B}_{pu} u_p(t) + \mathcal{B}_{pd} d(t), \\ y(t) = \mathcal{C}_p x_p(t) \end{cases} \tag{64}$$

with $\mathcal{A}_p,\ \mathcal{B}_{pu},\ \mathcal{B}_{pd},\ \mathcal{C}_p$ real matrices of appropriate dimensions, $x_p(t) \in \mathbb{R}^{n_p}$ the state of the plant, $u_p(t) \in \mathbb{R}^{n_u}$ and $d(t) \in \mathbb{R}^{n_d}$ the control input and the input disturbances, respectively, and $y(t) \in \mathbb{R}^{n_y}$ the plant output, at time $t \in \mathbb{R}_{\geq 0}$. The nonlinear controller ϕ is of the general form

$$\phi: \begin{cases} x_\phi[k] = f(y[k], y[k-1], x_\phi[k-1]), \\ u_p[k] = h(x_\phi[k]) \end{cases} \tag{65}$$

with $f : \mathbb{R}^{n_y} \times \mathbb{R}^{n_y} \times \mathbb{R}^{n_\phi} \to \mathbb{R}^{n_\phi}$, $h : \mathbb{R}^{n_\phi} \to \mathbb{R}^{n_y}$, and $x_\phi[k] \in \mathbb{R}^{n_\phi}$, $u_p[k] \in \mathbb{R}^{n_u}$, $y[k] \in \mathbb{R}^{n_y}$ denoting its state, output and input, respectively, at discrete time $k \in \mathbb{N}$, corresponding to time instants $t = kT_s$ with T_s the sampling period, as before. For the interconnection in Fig. 6, we choose the state $x_{sd}(t) = [x_p^\top(t)\ \ x_\phi^\top(t)]^\top \in \mathbb{R}^n$. Note that $\dot{x}_\phi(t) = 0$, for $t \in [kT_s, (k+1)T_s)$. In this section we investigate ISS of the closed-loop system in Fig. 6, as defined in Definition 4 below.

Definition 4. *[21] The interconnection in Fig.6 is said to be input-to-state stable if there exists $\beta \in \mathcal{KL}$ and $\gamma \in \mathcal{K}$, such that for all $x_{sd}(t_0) \in \mathbb{R}^n$ and $\|d\|_\infty \leq \infty$,*

$$\|x_{sd}(t)\| \leq \beta(\|x_{sd}(t_0)\|, t - t_0) + \gamma(\|d\|_\infty), \quad \forall t \geq t_0. \tag{66}$$

Note that the class of systems described by (65) includes as a particular case HIGS-based controllers as shown in Fig. 7, consisting of a DT HIGS element and DT LTI controllers $\mathcal{C}_i,\ i \in \{1, 2, 3\}$.

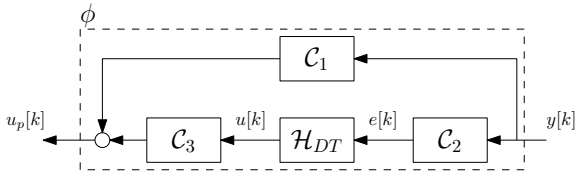

Fig. 7. The controller ϕ in the case of HIGS-based control.

Analysis of the system in Fig. 6 by following the DTD approach, requires a DT model of the plant $\mathscr{P}$ (64), which can be obtained via exact zero-order hold (ZOH) discretization of (64), leading to

$$\overline{\mathscr{P}}: \begin{cases} x_p[k] &= A_p x_p[k-1] + B_p u_p[k-1] + w[k-1], \\ y[k] &= C_p x_p[k] \end{cases} \tag{67}$$

with $A_p := e^{\mathcal{A}_p T_s},\ B_p := \int_0^{T_s} e^{\mathcal{A}_p \tau} d\tau \mathcal{B}_{pu},\ w[k-1] := \int_{(k-1)T_s}^{kT_s} e^{\mathcal{A}_p (kT_s - \tau)} \mathcal{B}_{pd} d(\tau) d\tau,\ C_p := \mathcal{C}_p$. Considering (67), we obtain the exact DT model

$$\begin{aligned} x_{sd}[k] &= \begin{bmatrix} A_p x_p[k-1] + B_p h(x_\phi[k-1]) + w[k-1] \\ f(C_p x_p[k], C_p x_p[k-1], x_\phi[k-1]) \end{bmatrix}, \\ y[k] &= \begin{bmatrix} C_p & 0 \end{bmatrix} x_{sd}[k] \end{aligned} \tag{68}$$

with $x_{sd}[k] = \begin{bmatrix} x_p^\top[k]\ x_\phi^\top[k] \end{bmatrix}^\top$ for the system in Fig. 6.

Using this exact model, we can formulate a corollary of Theorem 6 in [21], which can be used for concluding (CT) ISS of the sampled-data system under consideration, based on DT ISS of (68).

Corollary 1. *Suppose the DT system* (68) *is ISS with respect to the DT disturbance w. Then, the sampled-data system in Fig. 6, is ISS with respect to the CT disturbance d, in the sense of Definition 4.*

Proof. In between sampling instances, the system dynamics are linear since $\dot{x}_\phi(t) = \dot{u}_p(t) = 0$ for $t = (k-1)T_s + \lambda T_s$, $0 < \lambda < 1$ (due to ZOH), and thus the inter-sample behavior of states $x_{sd}(t) = [x_p^\top(t)\ x_\phi^\top(t)]^\top$ can be readily computed and shown to satisfy the boundedness property

$$\|x_{sd}(t)\| \leq \gamma_1(\|x_{sd}((k-1)T_s)\|) + \gamma_2(\|d\|_\infty) \tag{69}$$

for all $t \in [(k-1)T_s\ \ T_s]$, $k \in \mathbb{N} \setminus \{0\}$ and $\gamma_1, \gamma_2 \in \mathcal{K}_\infty$. Moreover, note that for $(k-1)T_s \leq t \leq kT_s$, $\|w[k-1]\|_\infty \leq c\|d\|_\infty$, with $c = \int_{(k-1)T_s}^{kT_s} \|e^{\mathcal{A}_p (kT_s - \tau)} \mathcal{B}_{pd}\|_\infty d\tau = \int_0^{T_s} \|e^{\mathcal{A}_p (T_s)} \mathcal{B}_{pd}\|_\infty d\tau$. Thus ISS of the DT system (68) with respect to w, implies its ISS with respect to the CT disturbance d. It follows now from Theorem 6 of [21], that the boundedness property (69), and ISS of (68) with respect to the DT disturbance w, implies ISS of the sampled-data system in Fig. 6 with respect to the CT disturbance d. □

For the case where ϕ is a HIGS-based controller as in Fig. 7, (68) is given by (19) or (23). Thus, as a result of Corollary 1, one may conclude ISS of the resulting sampled-data HIGS-controlled system using Theorem 2 and Theorem 3 or Theorem 4.

Preprint submitted to Automatica
Received November 20, 2023 08:38:48 Pacific Time

Remark 1. *Let us shortly note that while Corollary 1 builds on the results from [21] and uses a similar line of thought, our setting is slightly different from [21] in the sense that while in the configuration of Fig. 6, we consider linear CT systems controlled by DT nonlinear controllers, the work in [21] considers CT nonlinear systems controlled by linear DT controllers.*

Remark 2. *For a stabilizing controller of* (64) *to exist, stabilizability of* $(\mathcal{A}_p, \mathcal{B}_{pu})$ *as well as detectability of* $(\mathcal{A}_p, \mathcal{C}_p)$ *are required. Moreover, as shown in [4], in order to avoid the loss of these properties as a result of sampling, and thus for the existence of a DT stabilizing controller of* (64)*, the sampling period* T_s *should be non-pathological (see [4] for a detailed exposition on this topic) with respect to* $\mathcal{A}_p$*. Interestingly, note that, as shown in [22], in high precision motion control applications (forming a main area of application for HIGS-based control), the sampling is non-pathological for all* $T_s \in \mathbb{R}_{>0}$*.*

6 Numerical Example

In this section, we present a numerical example illustrating and comparing the different stability criteria presented in Section 4. The reader interested in time and frequency-domain simulations/experiments of successful applications of HIGS-based control improving over LTI control, is referred to [5, 15, 28, 32, 35]. Moreover [31, 33] it is shown how HIGS-based controllers overcome fundamental limitations of LTI control.

Consider the interconnection in Fig. 6, where $\mathscr{P}$ is a mass-spring-damper system with transfer function

$$\mathscr{P}(s) = \frac{1}{ms^2 + bs + k} \tag{70}$$

and mass $m = 1$ kg, damping coefficient $b = 0.0564$ Ns/m and stiffness coefficient $k = 1$ N/m. Moreover, the controller ϕ is as depicted in Fig. 7, with $\mathcal{C}_1(z) = 0$, $\mathcal{C}_2(z) = 1$ and $\mathcal{C}_3(z) = C(z)$ a linear lead filter, obtained by discretization of $C(s) = 1.4\frac{s+5}{s+6.95}$, using zero-pole matching [9]. Let us first consider a sampling time of $T_s = 0.001s$ (also used for the discretization of $C(s)$). To evaluate ISS of the DT closed-loop system using Theorem 2, note that the poles of the linear part of the system $P_{\text{lin}}(z) = P(z)C(z)$, with $P(z)$ the ZOH discretization of (70), are within the unit circle and thus condition i) in Theorem 2 is satisfied. Checking condition ii) in Theorem 2, amounts to inspecting the Nyquist diagram of $P_{\text{lin}}(e^{j\omega})$ as shown in Fig. 8, from which it follows that the closed-loop system is guaranteed to be ISS for any $\omega_h \in (0, \infty)$ and $k_h \leq 0.12$, by Theorem 2. Indeed, 0.12 is the maximal k_h value for which the Nyquist diagram in Fig. 8 falls to the right side of the vertical line passing

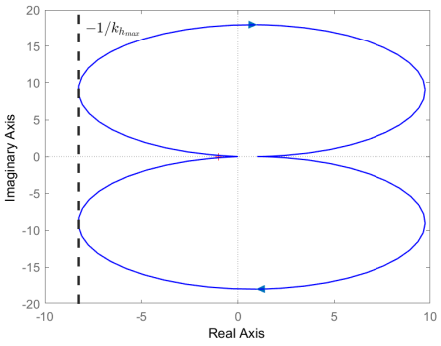

Fig. 8. Nyquist diagram of $P(z)C(z)$.

through $\frac{-1}{k_h} + j0$, in the complex plane, and thus satisfies condition ii) in Theorem 2.

In addition, the results obtained from Theorem 3 using LMI-based ISS guarantees for the case where $\mathcal{H}_{DT}$ is given by (38) , are portrayed in Fig. 9a as a function of the number N of partitions, $N \in \{1, 2, 4\}$. Note that Fig. 9a also shows the range of parameters for which the system is estimated to be ISS based on extensive time-series simulations. As it can be seen in Fig. 9a, by using

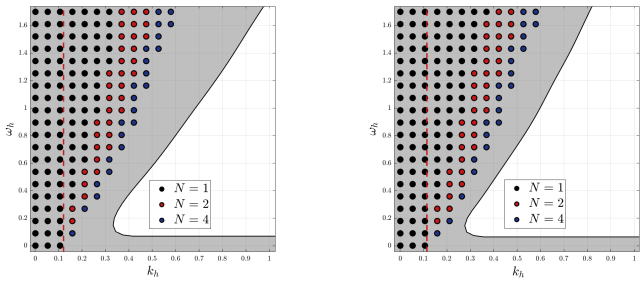

(a) (b)

Fig. 9. ISS region found by time-series simulations ■, ISS (k_h, ω_h) values returned by Theorem 3 (as a function of the number of partitions N), the k_h value obtained from Theorem 2 —, for a sampling time of (a) $T_s = 0.001s$, and (b) $T_s = 0.1s$.

Theorem 3, one concludes stability of (19) for a range of (k_h, ω_h) well beyond the values found by application of the frequency-domain conditions in Theorem 2, the latter indicated by the area to the left of the dashed (red) line. This is indeed expected as a result of Theorem 5 and the discussions in Section 4.4. To illustrate the effect of the sampling period, Fig. 9b portrays the analysis results obtained with a sampling time of $T_s = 0.1s$. Note that for $T_s = 0.1s$, the simulation-based estimated ISS region (the grey area) is smaller than for $T_s = 0.001s$. This indicates the general need for the analysis tools presented in this paper as pure CT analysis (see for example [6]) completely ignores the role of sampling, which in

Preprint submitted to Automatica
Received November 20, 2023 08:38:48 Pacific Time

turn could cause wrong conclusions regarding stability. Let us also make the observation that even with a single quadratic Lyapunov function, i.e., for $N = 1$, Theorem 3 provides a feasible range of (k_h, ω_h) values extending well beyond those obtained by Theorem 2, which indicates the strength of the relaxation terms introduced in Theorem 3.

The results obtained from application of Theorem 4 for the case where $\mathcal{H}_{DT}$ is given by (17) are presented in Fig. 10. Similar observations as in the case of Fig. 9 can

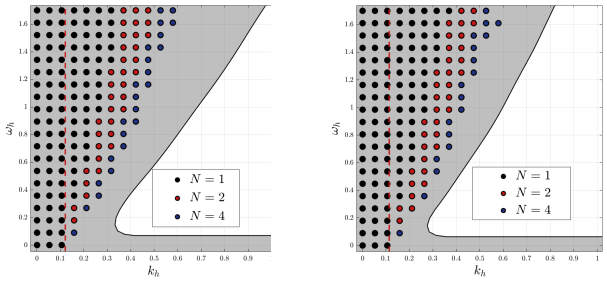

(a) (b)

Fig. 10. ISS region found by time-series simulations ■, ISS (k_h, ω_h) values returned by Theorem 4 (as a function of the number of partitions N), the k_h value obtained from Theorem 2 —, for a sampling time of (a) $T_s = 0.001s$, and (b) $T_s = 0.1s$.

be made. Namely, the results obtained from the LMIs are less conservative (even with $N = 1$) compared to the frequency-domain conditions, as expected due to Theorem 6. Moreover, the stability region is smaller for the case with slower sampling, thereby indicating the need for the tooling presented in this paper.

Lastly note that by virtue of Corollary 1, the results presented regarding stability of the closed-loop system in DT, are also valid for the SD system consisting of the CT plant (70) and the DT HIGS-based controllers.

7 Conclusions

In this paper, we have introduced two DT versions of HIGS, which preserve the main characteristics of CT HIGS, namely primary operation in the integrator mode while guaranteeing sign equivalence (sector boundedness) of its input-output pair. For the DT HIGS elements we have presented novel stability criteria that can be used to conclude ISS using (i) (measured) frequency response conditions and (ii) LMI-based conditions. We have also shown that satisfaction of these stability criteria imply ISS of sampled-data systems consisting of a CT plant and DT HIGS-based controllers (including the inter-sample behavior). While the frequency-domain criteria do not require parametric models and can be evaluated using easy-to-obtain frequency response data, we have formally proven that their satisfaction implies feasibility of a special case of the LMI-based conditions and thus are more conservative. This has been further illustrated by a numerical example showing that the LMIs are significantly less conservative than the frequency-domain criteria. Future research directions include reduction of the conservatism associated with the stability analysis, as well as transforming the presented stability criteria for synthesis of sampled-data HIGS-based controllers. Moreover, extensions of the work to cases with asynchronous sampling and hold elements and in the presence of delays is of interest. Lastly, in Theorems 5 and 6 we have shown that the satisfaction of the frequency-domain conditions in Theorem 2 are sufficient for the feasibility of the LMIs in Theorems 3 and 4. An interesting future direction of research is to investigate whether the inverse implication also holds true.

References

[1] V. Acary and B. Brogliato. *Numerical methods for nonsmooth dynamical systems: applications in mechanics and electronics*. Springer Science & Business Media, 2008.

[2] B. Bamieh and J Pearson. A general framework for linear periodic systems with applications to H_∞ sampled-data control. *IEEE transactions on automatic control*, 37(4):418–435, 1992.

[3] B. Brogliato, R. Lozano, B. Maschke, and O. Egeland. Dissipative systems analysis and control. *Theory and Applications*, 2:2–5, 2007.

[4] T. Chen and B. Francis. *Optimal sampled-data control systems*. Springer, 1995.

[5] D.A. Deenen, M.F. Heertjes, W.P.M.H. Heemels, and H. Nijmeijer. Hybrid integrator design for enhanced tracking in motion control. In *2017 American Control Conference*, pages 2863–2868. IEEE, 2017.

[6] D.A. Deenen, B. Sharif, S.J.A.M. van den Eijnden, H. Nijmeijer, W.P.M.H. Heemels, and M.F. Heertjes. Projection-Based Integrators for Improved Motion Control: Formalization, Well-posedness and Stability of Hybrid Integrator-Gain Systems. *Automatica*, 133:109830, 2021.

[7] G. Ferrari-Trecate, F.A. Cuzzola, D. Mignone, and M. Morari. Analysis of discrete-time piecewise affine and hybrid systems. *Automatica*, 38(12):2139–2146, 2002.

[8] B. Francis and T. Georgiou. Stability theory for linear time-invariant plants with periodic digital controllers. *IEEE transactions on Automatic Control*, 33(9):820–832, 1988.

[9] G. F. Franklin, J. D. Powell, and M. L. Workman. *Digital control of dynamic systems*, volume 3. Addison-wesley Reading, MA, 1998.

[10] L. Grüne and C.M. Kellett. ISS-Lyapunov functions for discontinuous discrete-time systems. *IEEE Transactions on Automatic Control*, 59(11):3098–3103, 2014.

[11] L. Han, A. Tiwari, M. K. Camlibel, and J.S. Pang. Convergence of time-stepping schemes for passive and extended linear complementarity systems. *SIAM Journal on Numerical Analysis*, 47(5):3768–3796, 2009.

[12] W. P. M. H. Heemels, V. Sessa, F. Vasca, and M. K. Camlibel. Computation of periodic solutions in maximal monotone dynamical systems with guaranteed consistency. *Nonlinear Analysis: Hybrid Systems*, 24:100–114, 2017.

Preprint submitted to Automatica
Received November 20, 2023 08:38:48 Pacific Time

[13] W.P.M.H. Heemels, G.E. Dullerud, and A.R. Teel. L2-gain analysis for a class of hybrid systems with applications to reset and event-triggered control: A lifting approach. *IEEE Trans. Automat. Contr.*, 61:2766–2781, 2016.

[14] W.P.M.H. Heemels and A. Tanwani. Existence and completeness of solutions to extended projected dynamical systems and sector-bounded projection-based controllers. *IEEE Control Systems Letters*, 7:1590–1595, 2023.

[15] M.F. Heertjes, S.J.A.M. van den Eijnden, B. Sharif, W.P.M.H. Heemels, and H. Nijmeijer. Hybrid integrator-gain system for active vibration isolation with improved transient response. *IFAC-PapersOnLine*, 52(15):454–459, 2019.

[16] Z. Jiang and Y. Wang. Input-to-state stability for discrete-time nonlinear systems. *Automatica*, 37(6):857–869, 2001.

[17] H.K. Khalil. *Nonlinear systems*. 3^{rd} edition, Prentice hall, Upper Saddle River, 2002.

[18] M. Larsen and P. V. Kokotović. A brief look at the Tsypkin criterion: from analysis to design. *Int. J. Adapt. Control and Signal Processing*, 15(2):121–128, 2001.

[19] D. Nešić, L. Zaccarian, and A. R. Teel. Stability properties of reset systems. *Automatica*, 44(8):2019–2026, 2008.

[20] D. Nešić, A.R. Teel, and P.V. Kokotović. Sufficient conditions for stabilization of sampled-data nonlinear systems via discrete-time approximations. *Syst. Control Lette.*, 38(4):259–270, 1999.

[21] D. Nešić, A.R. Teel, and E.D. Sontag. Formulas relating $\mathscr{KL}$ stability estimates of discrete-time and sampled-data nonlinear systems. *Syst. Control Lett.*, 38(1):49–60, 1999.

[22] T. Oomen, M. van de Wal, and O. Bosgra. Design framework for high-performance optimal sampled-data control with application to a wafer stage. *International Journal of Control*, 80(6):919–934, 2007.

[23] J.S. Pang, V. Kumar, and P. Song. Convergence of time-stepping method for initial and boundary-value frictional compliant contact problems. *SIAM journal on numerical analysis*, 43(5):2200–2226, 2005.

[24] A. Rantzer. On the Kalman—Yakubovich—Popov lemma. *Systems & control letters*, 28(1):7–10, 1996.

[25] B. Sharif, D.W.T. Alferink, M.F. Heertjes, H. Nijmeijer, and W.P.M.H. Heemels. A discrete-time approach to analysis of sampled-data hybrid integrator-gain systems. In *IEEE Conference On Decision and Control, Cancun, Mexico*, pages 7612–7617, 2022.

[26] B. Sharif, M. Heertjes, H. Nijmeijer, and W.P.M.H. Heemels. On the equivalence of extended and oblique projected dynamics with applications to hybrid integrator-gain systems. In *American Control Conference (ACC) 2021, New Orleans, USA*, pages 3434–3439, 2021.

[27] B. Sharif, M.F. Heertjes, and W.P.M.H. Heemels. Extended projected dynamical systems with applications to hybrid integrator-gain systems. In *2019 IEEE Conference on Decision and Control (CDC)*, pages 5773–5778, 2019.

[28] K. Shi, N. Nikooienejad, I.R. Petersen, and S. O. R. Moheimani. A negative imaginary approach to hybrid integrator-gain system control. In *IEEE Conference On Decision and Control, Cancun, Mexico*, pages 1968–1973, 2022.

[29] E.D. Sontag. Smooth stabilization implies coprime factorization. *IEEE Transactions on Automatic Control*, 34(4):435–443, 1989.

[30] D. E. Stewart. Convergence of a time-stepping scheme for rigid-body dynamics and resolution of painlevé's problem. *Archive for Rational Mechanics and Analysis*, 145(3):215–260, 1998.

[31] S.J.A.M. van den Eijnden, M.F. Heertjes, W.P.M.H. Heemels, and H. Nijmeijer. Hybrid integrator-gain systems: A remedy for overshoot limitations in linear control? *IEEE Control Systems Letters*, 4:1042 – 1047, 2020.

[32] S.J.A.M. van den Eijnden, M.F. Heertjes, and H. Nijmeijer. Robust stability and nonlinear loop-shaping design for hybrid integrator-gain-based control systems. In *2019 American Control Conference*, pages 3063–3068. IEEE, 2019.

[33] D. van Dinther, B. Sharif, S. J. A. M. van den Eijnden, H. Nijmeijer, M. F. Heertjes, and W. P. M. H. Heemels. Overcoming performance limitations of linear control with hybrid integrator-gain systems. In *IFAC Conf. Anal. Design of Hybrid Systems (ADHS), Brussels, Belgium*, pages 289–294, 2021.

[34] L. Zaccarian, D. Nešić, and A.R. Teel. First order reset elements and the Clegg integrator revisited. In *2005 American Control Conference*, pages 563–568. IEEE, 2005.

[35] G. Zhao and C. Hua. A hybrid switching control approach to consensus of multiagent systems. *IEEE Transactions on Cybernetics*, 52(10):11133–11143, 2022.

Preprint submitted to Automatica
Received November 20, 2023 08:38:48 Pacific Time